

# Compact Circularly Polarized Monopole Antenna Using Characteristic Mode Analysis

Samineni Peddakrishna<sup>1,\*</sup>, Lulu Wang<sup>2</sup>, Vamshi Kollipara<sup>1</sup>, Jayendra Kumar<sup>1</sup>

<sup>1</sup>School of Electronics Engineering, VIT-AP University, Amaravati, India

<sup>2</sup>Biomedical Device Innovation Center, Shenzhen Technology University, Shenzhen, China

Received 12 December 2022; received in revised form 18 January 2023; accepted 30 January 2023

DOI: <https://doi.org/10.46604/peti.2023.11274>

## Abstract

This study aims to design a circularly polarized compact antenna using characteristic mode analysis (CMA). The proposed antenna consists of a substrate with a slotted annular ring-shaped patch and partial ground. The excitation position of the antenna and its optimal dimensions are determined through the analysis of different operation modes with CMA. After that, an optimized antenna is designed, and an antenna prototype is fabricated for validation. The experimental results show that the reflection coefficient achieves a -10dB impedance bandwidth of 6.85 GHz, a 3dB-axial ratio bandwidth of 0.7 GHz, and a peak gain of 3.2 dBi. These characteristics agree with simulations and make the circularly polarized compact antenna suit for C-band and sub-6 GHz 5G wireless applications.

**Keywords:** axial ratio, characteristic mode analysis, circular polarization, monopole antenna, wideband

## 1. Introduction

In recent years, circularly polarized (CP) antennas have gained popularity for wireless communication applications, such as microwave and millimeter waves. Using a CP antenna can minimize the effects of multipathing and degradation. CP antennas provide more flexibility in the transmitter and receiver configurations than linearly polarized antennas [1]. Because of these advantages, planar CP antennas have become popular for various applications such as wireless microwave access, wireless local area networks, navigation, and satellite communications.

A circular polarization wave is generally produced by exciting two orthogonal modes with quadrature phase and equal magnitudes. To excite orthogonal modes, the crossed dipole antenna [2], dielectric resonator antenna (DRA) [3], and slotted antenna [4] were developed. The cross-dipole antenna was designed for a 2.45 GHz industrial, scientific, and medical band on a double-layer printed circuit board [2]. A quarter wavelength distance ground plane is required for the effective radiation, but the size is increased. Varshney et al. [3] proposed the DRA which provides a wider circular polarization bandwidth. DRAs are larger and more complex than microstrip patch antennas. Seyyedrezaei et al. [4] proposed a novel slot antenna design for 5G applications operating at sub-6 GHz. However, this design has a low axial ratio bandwidth (ARBW) and low impedance bandwidth (IPBW).

The excitation of CP waves by printed monopole antennas poses a significant challenge for many researchers. Monopole antennas were generally used to increase IPBW. However, due to the less small horizontal component of the radiation in the far field, it is a challenge to design circular polarization [5]. To achieve circular polarization antennas, the printed monopole antennas with elliptical [6], Chifre-shaped [7], parasitic strip [8], and C-shaped [9] were developed. The above configurations [6-9] of CP-printed antennas have significant physical areas and complex features.

---

\* Corresponding author. E-mail address: [krishna.samineni@gmail.com](mailto:krishna.samineni@gmail.com)

Other studies [10-13] investigated different compact configurations. Panahi et al. [10] designed a simple sickle-shaped CP antenna with a circular slotted ground plane and a dimension of  $0.29 \lambda \times 0.29 \lambda$  at the lowest operating frequency. Samsuzzaman et al. [11] proposed a hook-shaped branch and reversed unequal arm L-shaped microstrip-feed antenna with  $0.33 \lambda \times 0.33 \lambda$  dimensions. Alsariera et al. [12] presented an L-shaped monopole and inverted L-strip antenna design to achieve wide impedance and ARBW.

In addition, Manohar and Chaudhary [13] proposed another compact design based on a triangular monopole antenna that operates in the frequency range from 2 GHz to 9 GHz with wide impedance and ARBW. These antennas are typically tuned by changing patch shapes and feed positions through parameter sweeps. Moreover, these methods do not provide physical insights into their design regarding the feed length, substrate, and optimization of the antenna structure.

To resolve this issue and provide physical insight, characteristic mode analysis (CMA) was utilized in antenna design configurations [14-15]. The resonant behavior of antenna structures can be analyzed by the CMA technique using a source-free method, which decomposes a full wave current mode into individual modes [16]. As a result, undesired modes will be suppressed, allowing the excitation of desired modes to gain physical insights [17]. Kollipara and Peddakrishna [18] analyzed the characteristic modes of antenna design to achieve circular polarization. Several research groups have evaluated CMA-based methodologies with and without metasurfaces. Among these methodologies, an asymmetric U-slot patch antenna [19] and two crossed dipole antennas [20] were respectively given insight into the suppression of undesired modes and accomplishment of quadrature phase shift. The ARBW in these designs is very narrow.

Other designs for circular polarization such as I-shaped slot antennas [21], annular ring microstrip feed with asymmetric slot [22], and C-shaped monopole patch with a C-shaped grounded aperture [23] exhibit quadrature phase shift characteristics with a CMA. However, the effect of feed length and performance of substrate thickness was not addressed adequately. The following approaches are presented to address the issue:

- (1) An antenna with circular polarization capabilities is designed using a slotted annular ring monopole antenna based on the CMA concept.
- (2) CMA is used to analyze and optimize the slotted annular ring monopole antenna's feed point, feed length, substrate dimensions, and thickness before excitation.
- (3) Circular polarization is characterized by a magnitude of the modal significance (MS) and a quadrature phase difference for the characteristic angle (CA) between modes.

Computer simulation Technology (CST) is used to analyze the resonance behavior, the surface currents, and the radiation characteristics at different stages of the CMA without an excitation of the feed. The evaluated antenna results achieved IPBW ranging from 3.3 GHz to 9.4 GHz and ARBW ranging from 3.3 GHz to 4.0 GHz.

The remainder of this paper is organized as follows: Section 2 provides the required characteristic mode (CM) parameters to classify the modes in the antenna design, tracked by the design methodology using CMA. Section 3 analyzes the annular ring patch in different stages, annular ring operating mechanism, feed-line width, substrate thickness, and ground plane length. Section 4 discusses the parameters of an excited antenna and their validation. Finally, Section 5 concludes the proposed work.

## **2. CM Parameters and Design Methodology**

This section introduces the valuable parameters and design methodologies of CMA that are useful during the antenna design procedure. It specifically focuses on the importance of CM parameters, the application of extracting model behavior from the antenna design, and optimized approaches to meet the desired parameters.

2.1. CM parameters

A CMA begins with determining the modal behavior of the CM parameters, which contain information about resonance. Essentially, the analysis can be described as an eigenvalue ( $\lambda_n$ ) [14]. The eigenvalue is a helpful parameter for providing information about modes. In other words, it is the total field energy stored within a radiating structure. In addition to the eigenvalue, two additional parameters MS and CA derived from it are also taken into account to extract the modal behavior, which can be expressed as:

$$MS = \frac{1}{|1 + j\lambda_n|} \tag{1}$$

$$\varnothing_n = 180^\circ - \tan^{-1}(\lambda_n) \tag{2}$$

The MS is a valuable parameter that can transform a much higher eigenvalue  $[-\infty, +\infty]$  into a range of  $[0, 1]$  to visualize the resonance behavior better. In addition, the CA ( $\varnothing_n$ ) parameter indicates the phase lag between the electric field and the real characteristic current. It helps identify the phase lag between different modes of operation. MS and CA parameters can quickly identify resonance and phase behavior between the modes; hence, these parameters are instrumental in identifying a structure’s circular polarization behavior [18].

2.2. Antenna design methodology using CMA

In the CMA analysis, resonance information was extracted from CM parameters, determined from the intended structure, and completely independent of the excitation source. However, practical radiating antennas would generally consider the effect of sources. Therefore, Fig. 1 shows the design flow of three phases for an antenna based on CMA, which are modal analysis, CMA design with excitation, and desired parameters verification.

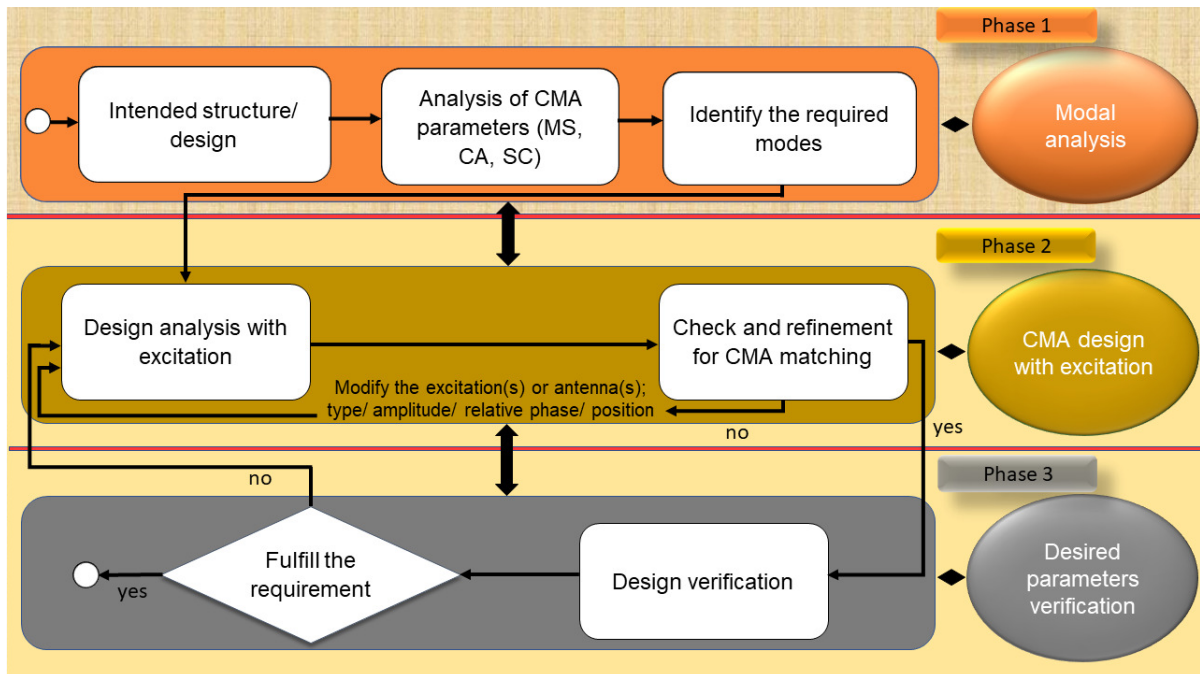


Fig. 1 CMA design procedure of a typical antenna

As part of the initial phase of the design flow, modal analysis was carried out to determine the modal behavior of the geometry. Modal means there is no need for any excitation or analysis through CMs. During this phase, resonant modes that were naturally supported by the geometry were extracted within the desired frequency range. The modal currents or modal fields were considered to calculate each mode’s radiation pattern or radiation field. In addition, during this phase, it was possible to modify the structure to achieve the desired modal attributes, such as resonance, current, and field or pattern.

The second phase began with the system's excitation based on the selection of appropriate geometry and modes. In this stage, the antenna geometry would be examined to determine how the selected modes would be coupled during the CMA study. In addition to the characteristic parameters, modal decompositions can be used to evaluate how well each design excited the desired modes. This phase was iterative and consisted of modifying the antenna structure's size, shape, and excitation until a certain degree of modal excitation was achieved. Modal decompositions can be performed by calculating the modal excitation coefficient, the modal weighting coefficient, and the modal input power. In this case, the total current on the structure will form a set of orthogonal currents when the total current is assumed to be a linear superposition.

The final phase is a stage of verifying the desired parameter. In this case, outputs such as reflection coefficients, bandwidths, and gain for the entire design were examined. Then, if the desired parameters are met, the design is completed. Otherwise, the structure will have to be modified and revised in the second phase. In this way can evaluate all stages of the antenna design for enhanced performance.

### 3. Proposed Design Analysis Using CMA

Fig. 2 depicts the proposed annular ring patch modification progression through CMs. This design started with a basic annular ring employing a perfect electric conductor (PEC) with a thickness of zero and without considering the substrate, as illustrated in Fig. 2(a). A cavity model was performed on the outer and inner radius of the Annular ring @1 to understand the effects of the dominant modal behavior of the initial annular ring. Based on the cavity equation [24], the dominant modes can be determined from:

$$f_{nm} = \frac{k_{nm}c}{2\pi\sqrt{\epsilon_{eff}}} \quad (3)$$

$$J'_n(kb)Y'_n(ka) - J'_n(ka)Y'_n(kb) = 0 \quad (4)$$

where  $k_{nm}$  is the root of the characteristic equation,  $c$  is the velocity of light in free space, and  $\epsilon_{eff}$  is the effective permittivity.  $J'_n(x)$  and  $Y'_n(x)$  are respectively the first and second kinds of Bessel functions, and the primes represent derivatives  $x$ . This results in the roots of the characteristic equation  $k_{nm}$  with different modes with the ratio of outer to the inner radius of 2, obtaining the value of 0.6673 for the fundamental mode [25]. Additionally, the resonance frequency of the proposed annular ring without a substrate ( $\epsilon_{eff} = 1$ ) was observed at around 8 GHz. Accordingly, this empirical equation satisfies the dominant frequency region of the proposed annular ring patch.

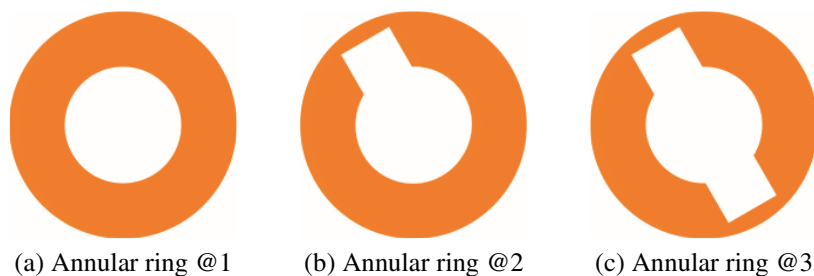


Fig. 2 Different stages of proposed annular ring evolution

To investigate this dominant behavior using CMA, the first five CMs from Mode 1 to Mode 5 of Annular ring @1 were analyzed using a CST-based integral equation solver and are presented in Fig. 3. Mode 1 to Mode 5 represents the first five CMs, obtained through mathematical analysis of the antenna's geometry, material properties, and operating frequency. The origin of the CMs is based on the solution of Maxwell's equations for the antenna structure (Antenna @1). These modes are determined based on the eigenvalues obtained from the analysis and are selected based on their strength and significance in contributing to the overall radiation pattern of the antenna.

The division of CMs into 5 modes is arbitrary and depends on the specific analysis being performed. The difference between the modes is in the pattern of current distribution and the resulting radiation characteristics. Each mode represents a unique pattern of current distribution on the antenna has its own resonant frequency and radiation pattern. The strength of each mode determines its contribution to the overall radiation pattern of the antenna. Mode 1 and mode 2 are dominant (greater than 0.707) from 7 GHz and attain a maximum of 9 GHz in the specified frequency range of interest. However, mode 1 to mode 5 has the same CA variation, as observed in Fig. 3(b), which does not contribute to generating circular polarization. Also, as shown in Fig. 3(a), the remaining modes from mode 3 to mode 5 are regarded as nonsignificant modes because the MS is less than 0.707. As observed from the characteristic mode, the Annular ring @1 generates significant degenerate modes. Thus, the effective length must differ in both x- and y- directions to distinguish the phase difference between two orthogonal modes.

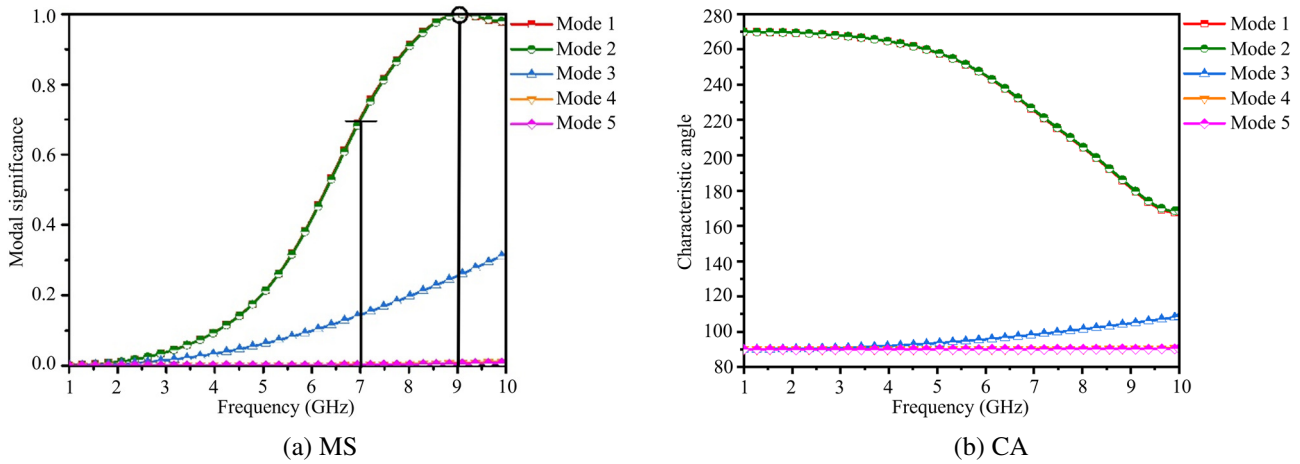


Fig. 3 Characteristic mode parameters of Annular ring @1

To alter the effective length in both directions, a rectangular patch was subtracted from the annular ring patch. A similar principle can be applied to other shapes, such as C-shaped [23] and U-shaped [26], in the same manner. To create a minor perturbation in an Annular ring @1, a symmetric square patch of  $4 \times 4 \text{ mm}^2$  was etched at the upper left part at an angle of around  $300^\circ$  in a clockwise direction to form an Annular ring @2, as shown in Fig. 2(b). Compared to the Annular ring @1, the rectangular slot extends the current path in the Annular ring @2, causing the resonant frequency to shift to a lower frequency. Fig. 4 illustrates the CMs of the Annular ring @2. From MS, it can be seen that the degenerated modes are split into two distinct modes.

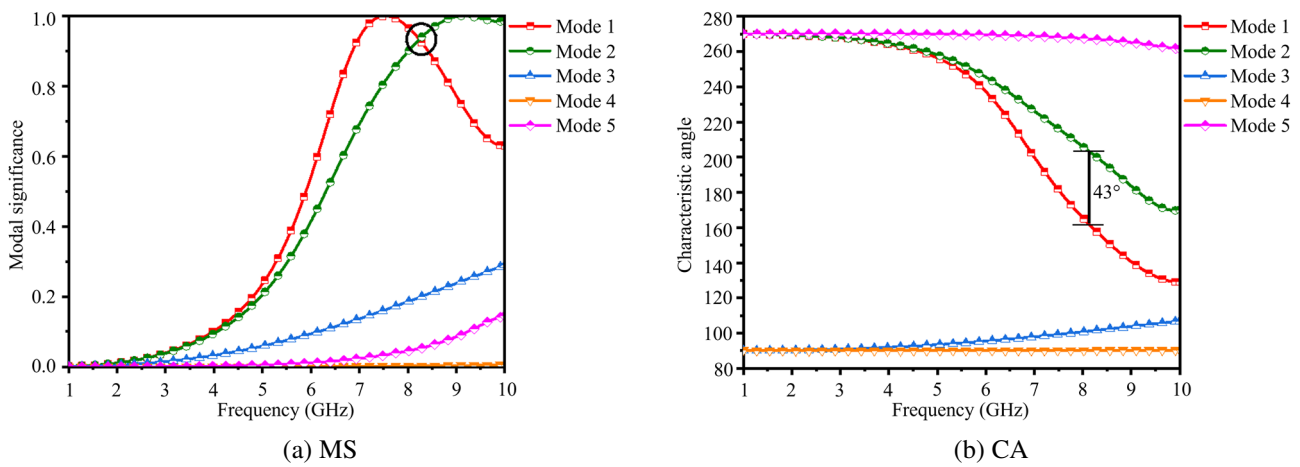


Fig. 4 Characteristic mode parameters of Annular ring @2

There is an intersection point between the first two modes at 8.24 GHz with an MS value of 0.93, which is essential for circular polarization. At the same time, they present a CA phase difference is  $43^\circ$ . To obtain further shifts in phase difference, another rectangular perturbation is made on the lower right side of the patch in an Annular ring @2 to form an Annular ring @3.

The current path was further extended, and the resonance frequency was further lowered. This approach increased the difference between two resonant frequency modes and improved the phase difference between two orthogonal modes to obtain circular polarization.

According to the CMs shown in Fig. 5, mode 1 is adjusted to the lower frequency of 6.40 GHz, while mode 2 maintains its resonance frequency at 9.09 GHz. The intersection point between modes 1 and 2 is observed at 7.27 GHz, with an MS value of 0.74 and a CA value of  $83^\circ$ . As shown in Fig. 5, the MS values for the remaining modes from mode 3 to mode 5 are less than 0.707, indicating that these modes are not significant. This observation is similar to the previous higher-order modes, as depicted in Fig. 4 for the Annular ring @2. After analyzing the CMs, the next step was to identify the feed position by observing the distribution of surface currents. By adjusting the angle in the fourth and second coordinates, the perturbation position could be changed and the optimal position was selected.

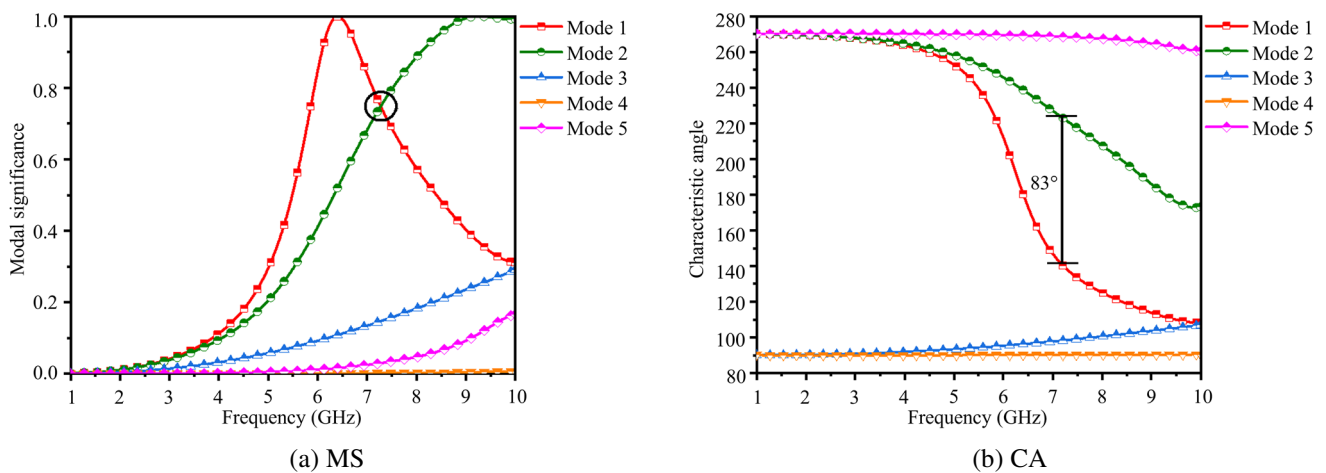


Fig. 5 Characteristic mode parameters of Annular ring @3

Fig. 6 depicts a surface current distribution to identify the placement of the feed point in an Annular ring @3. A surface current distribution for resonance modes at the intersection point of the Annular ring @3 was observed at frequencies of 6.40, 7.27, and 9.09. According to the maximum current distribution, both modes were excited properly if the feed point was highlighted with A, B, and C. Thus, the feed point was considered at the bottom of the Annular ring @3 for further analysis.

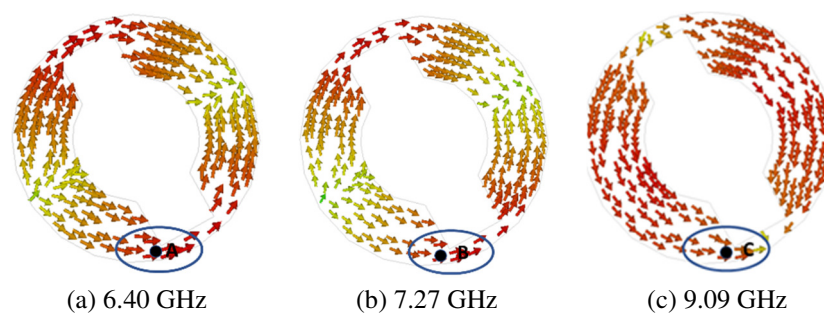


Fig. 6 Surface current distribution of Annular ring @3

Upon identification of the feed point and consideration of the feed dimensions, the CMA was further extended with different stages, such as stages 1, 2, and 3, as shown in Fig. 7. The first stage consists of an Annular ring @3 patch with a feed line without a substrate, while the second stage consists of a patch with a substrate. In the third stage, a patch is added to the substrate's opposite side from the one applied in the second step.

To better visualize the effect of the feed dimension, the optimized CMs of stage 1 are depicted in Fig 8. The MS results show that modes at 4.73 GHz, 6.56 GHz, and 9.90 GHz are the most significant modes. In addition, the CA at their intersection point of 5.91 GHz between modes 1 and 2 is  $90^\circ$ , and at 8.26 GHz between modes 2 and 5 is  $109^\circ$ .

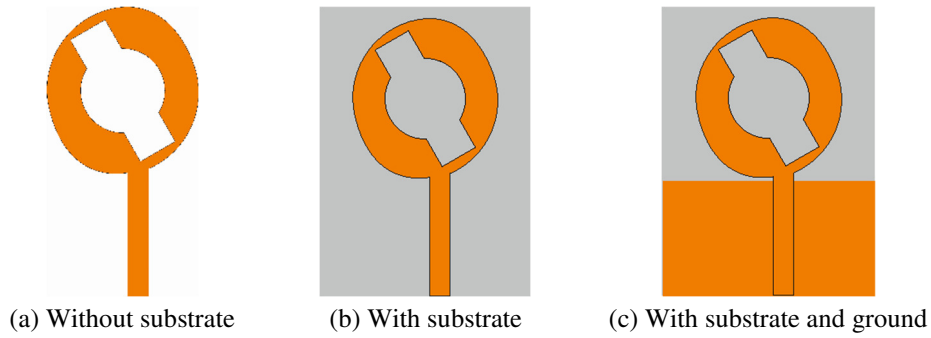


Fig. 7 Different stages of feed configurations

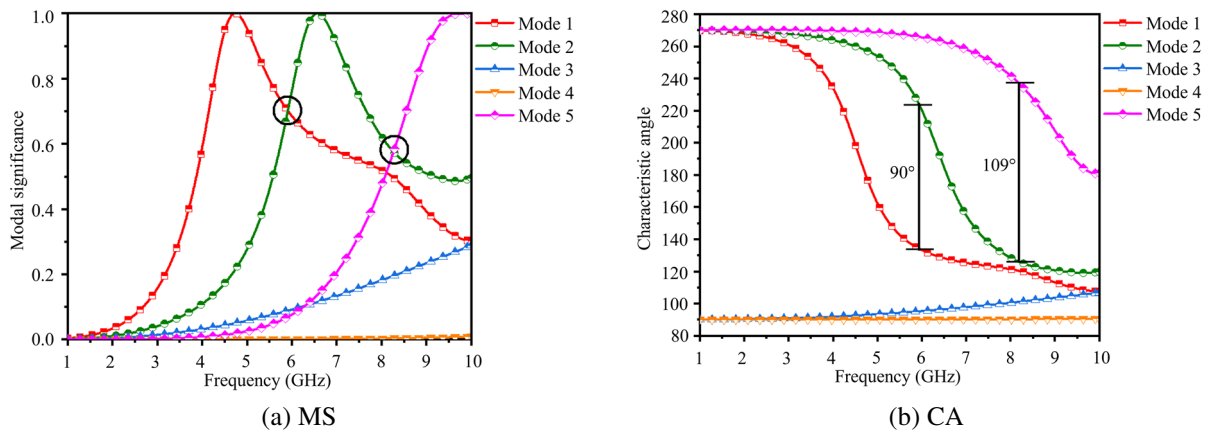


Fig. 8 Characteristic mode parameters of the annular ring with feed

Following the completion of stage 1, the CMA was analyzed for stage 2 design. To determine the substrate, a parametric analysis was conducted by varying the substrate dimensions. Fig. 9 shows the optimized results of MS and CA. The resonance modes are shifted to the lower frequency side without significantly changing the CA performance where the modes intersect. Among modes 1, 2, and 5, there is an intersection point at 4.94 GHz and 6.66 GHz, where the MS is 0.67 and 0.59, with a CA of 95° and 107°. It was observed that the resonance modes which correspond to modes 1, 2, and 5 are respectively at frequencies of 3.81 GHz, 5.54 GHz, and 8.36 GHz for wideband operation.

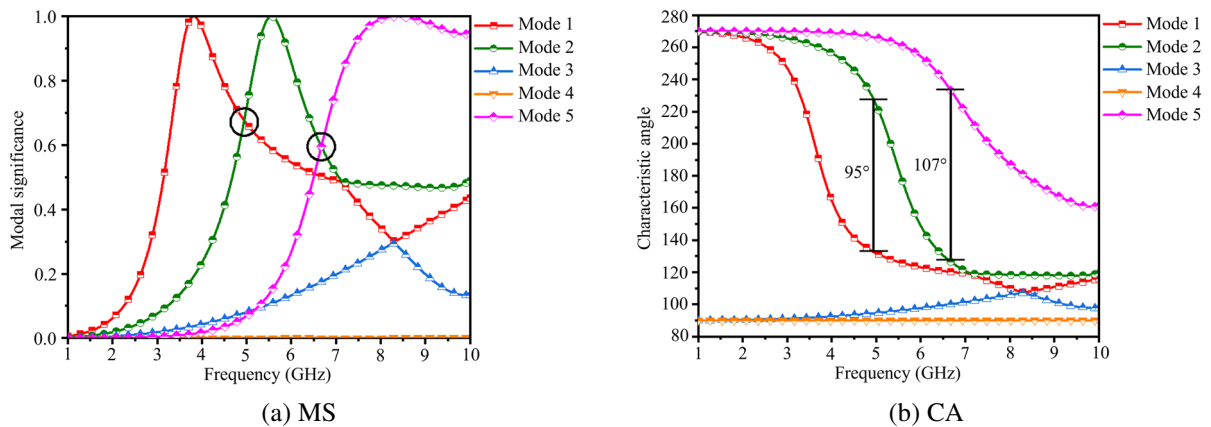


Fig. 9 Characteristic mode parameters of the patch with a substrate

After the stage 2 analysis, CMs were examined by applying a partial rectangular patch on the opposite side of the substrate. The partial ground plane was considered capable of supporting multiple modes of resonance, while a conventional ground plane can only support one mode of resonance [27]. Multiplicative closely spaced resonance modes ( $f_1, f_2, f_3, \dots, f_N$ ) can achieve a wide bandwidth, and this is the concept behind monopole structures' wide bandwidth. It brings the number of significant modes from three to four by providing a partial patch. Fig. 10 illustrates the results of the MS and CA. There were four resonant modes (1, 2, 4, and 5) at 3.14 GHz, 4.38 GHz, 5.74 GHz, and 7.05 GHz, respectively. In addition, the intersection

point between modes 1 and 2 is observed at 3.58 GHz with an MS of 0.707 and a CA of 90°. With this, circular polarization can be produced under two orthogonal modes having 90° phase differences of equal magnitude. Other intersecting points are observed between modes 2, 4, and 5 at 5.17 GHz and 6.64 GHz. However, the intersection points at 5.17 GHz and 6.64 GHz contributes only the wide IPBW with an MS of 0.8 and a CA of 73°; an MS of 0.92 and a CA of 43°.

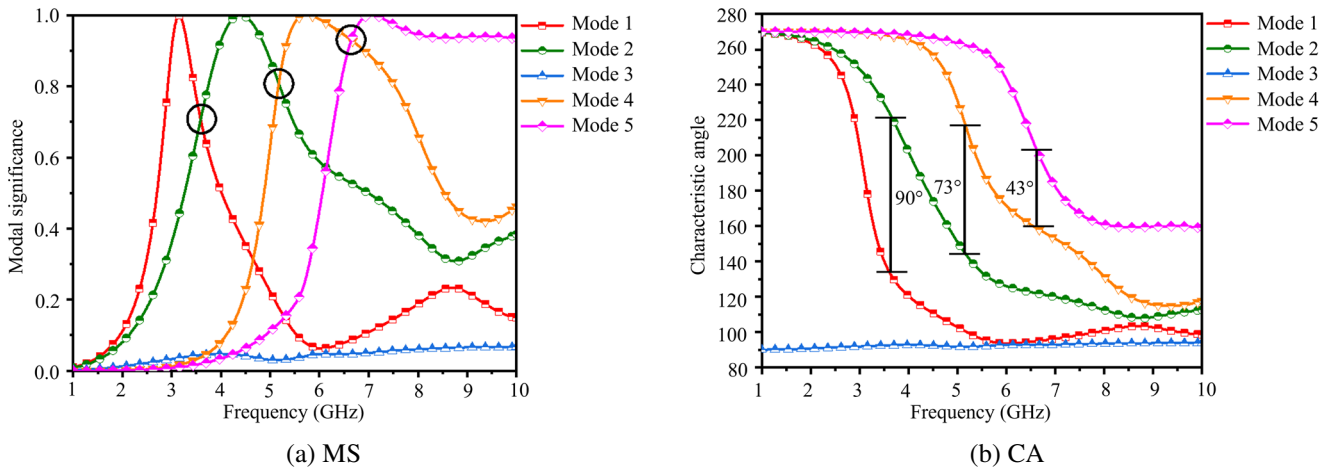


Fig. 10 Characteristic mode parameters of the patch with the partial ground plane

To understand the design approach, the optimized design’s characteristic currents, and radiation behavior were further analyzed using CMA. As part of the analysis, the design in stage 3 of Fig. 7 was considered, which consisted of an annular ring patch, a partial ground plane, a feed, and a substrate. The current distribution and radiation performance were analyzed at the intersecting mode frequencies of the design. These frequencies were 3.58 GHz, 5.17 GHz, and 6.64 GHz. According to Fig. 11, the maximum current for mode 1 ( $J_1$ ) is located towards the left of the annular ring, while the maximum orthogonal current for mode 2 ( $J_2$ ) is in the downward direction. The results indicate that modes 1 and 2 dominate in perpendicular directions with equal amounts of radiation.

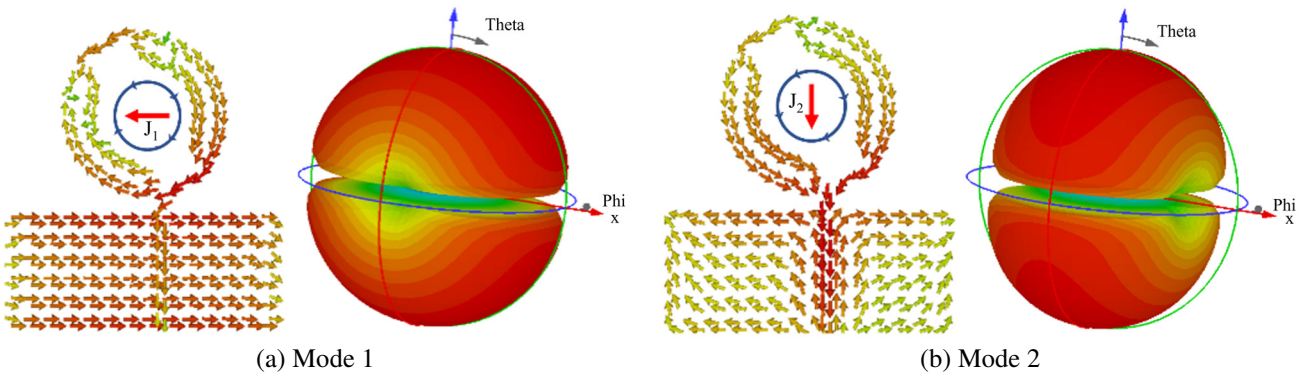


Fig. 11 Surface current and 3-D radiation pattern of modes at 3.58 GHz

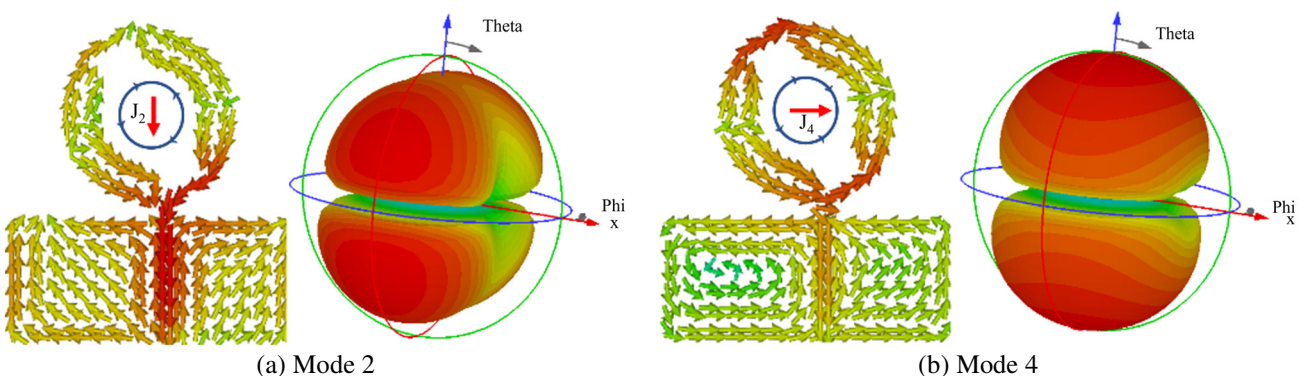


Fig. 12 Surface current and 3-D radiation pattern of modes at 5.17 GHz

Figs. 12-13 shows the current distribution and radiation performance at 5.17 GHz and 6.64 GHz. Mode 2 radiated less likely in the z-direction, whereas mode 4 radiated strongly in the z-direction. Furthermore, the current directions were predominantly offset from the z-direction. As shown in Fig. 13, both modes radiate in a broadside direction with uniform current distribution despite their difference in the quadrature phase.

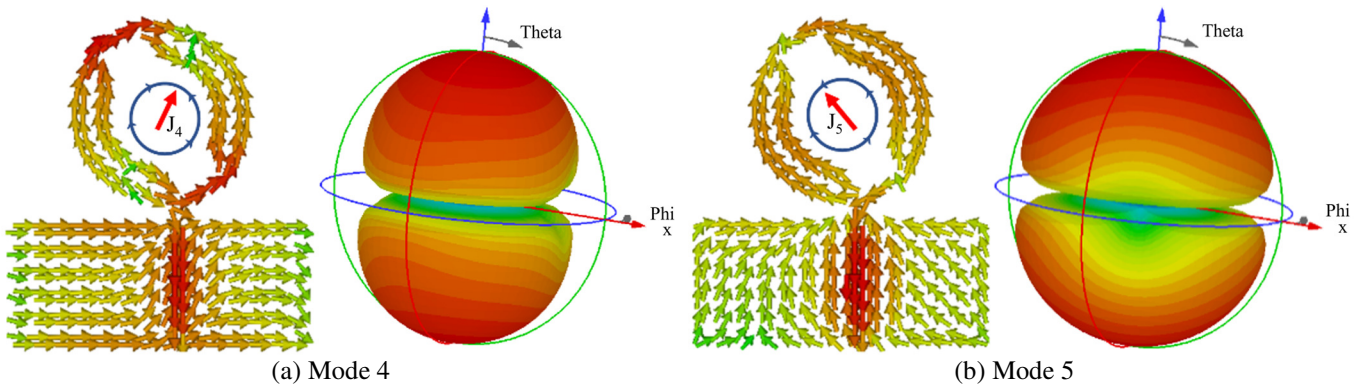


Fig. 13 Surface current and 3-D radiation pattern of modes at 6.64 GHz

#### 4. Proposed Antenna Analysis and Validation

Following the analysis of the CMs without external excitation, a validation analysis was conducted with excitation to determine whether the proposed CM approach is valid. This section describes the complete compact CP antenna design procedure with a slotted annular ring patch for broad impedance characteristics, including their validation. For this purpose, the antenna was designed using an FR-4 substrate with a thickness of 0.8 mm. The patch, along with the feed and ground plane, was respectively placed on the top and bottom sides of the substrate. The size of the antenna was  $22 \times 30 \times 0.8 \text{ mm}^3$ . Fig. 14 shows the design of the proposed antenna, and Table 1 shows the parameters of the proposed antenna.

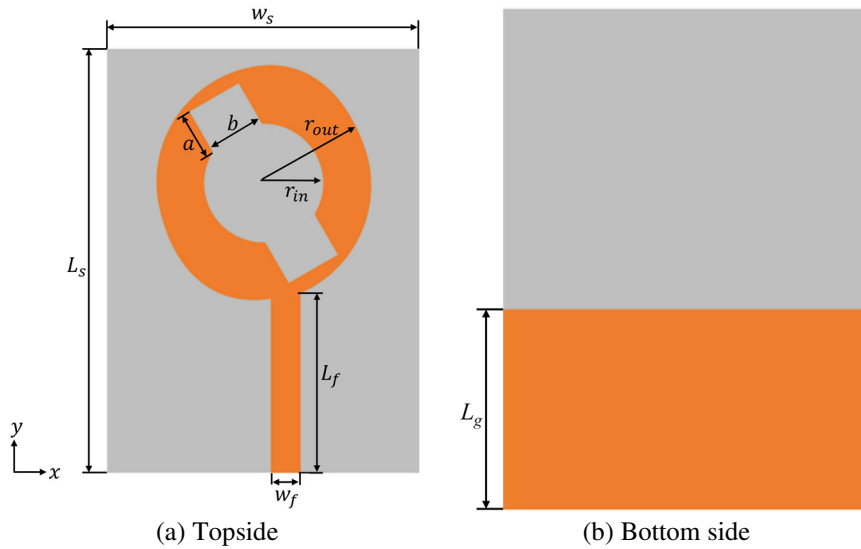


Fig. 14 Geometry of the proposed antenna

Table 1 Geometrical Parameters of the proposed antenna

Parameter	$W_s$	$L_s$	$L_g$	$a$	$b$	$r_{in}$	$r_{out}$	$L_f$	$W_f$
Value (mm)	22	30	12	4	4	4.2	8.2	13	2.1

Based on the above design and excitation, the IPBW and ARBW parametric analyses were performed for the substrate thickness, the partial ground plane length variation, and the feed width variation. A thickness ( $h_s$ ) variation was performed for the commercially available substrates ranging from 0.2 mm to 1.6 mm. Fig. 15 shows the reflection coefficient ( $S_{11}$ ) and axial ratio (AR) variation. The thickness changes from 0.2 to 1.6 mm, and the antenna IPBW increases and achieves a perfect

matching at 1.6 mm thickness. Simultaneously, the ARBW is reduced, and the ARBW is more with a thickness of 0.4 mm. Hence, to compensate for both results, the optimized thickness of the substrate was considered as 0.8 mm. This thickness provided satisfactory CP radiation in the specified band from CM analysis.

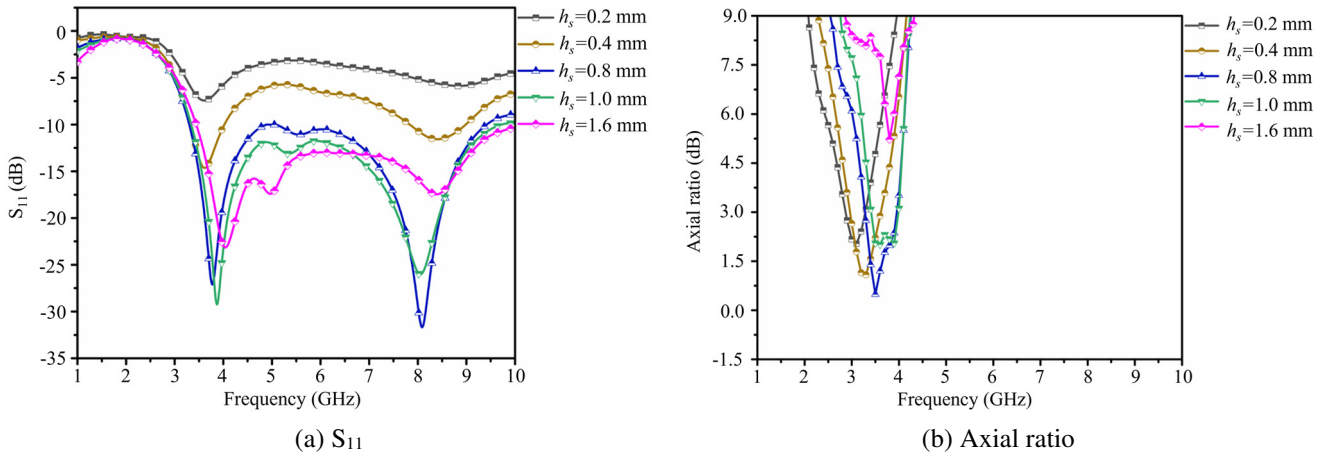


Fig. 15 Simulated results based on the thickness of the substrate

In the next step, a parametric analysis of ground length ( $L_g$ ) was performed and presented in Fig. 16. The analysis involved varying the parameter  $L_g$  in increments of 1 mm from 11 mm to 15 mm. As a result, the IPBW increased and the ARBW decreased. The ARBW was not even provided if the ground length exceeded 13 mm or less than 12 mm. During the CM analysis, the quadrature phase shift condition was not satisfied since the ground length was less and beyond the values mentioned above. Thus, to compensate for the IPBW and ARBW, the partial ground length was optimized for 12 mm.

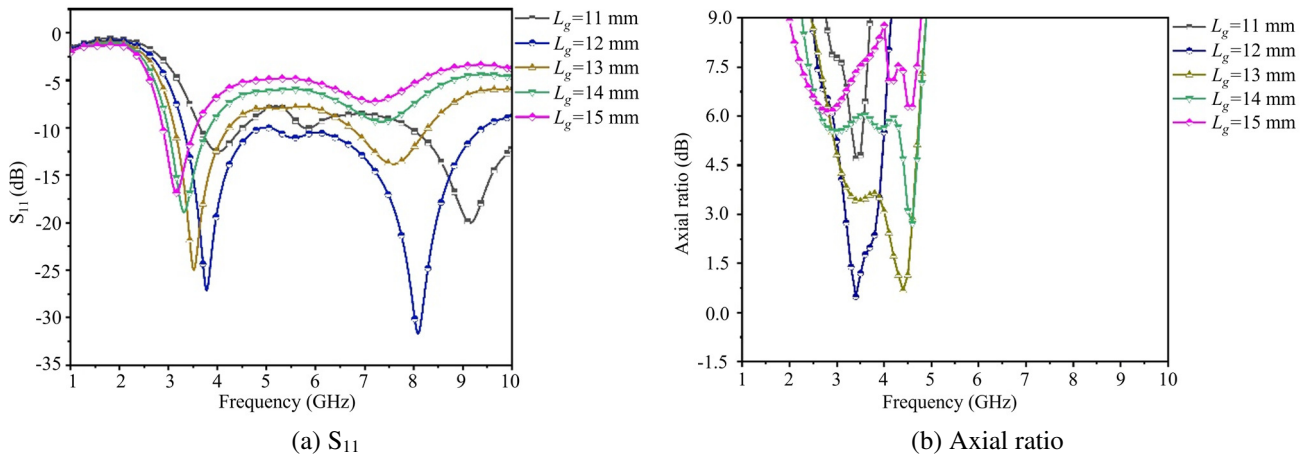


Fig. 16 Simulated results based on ground length variations

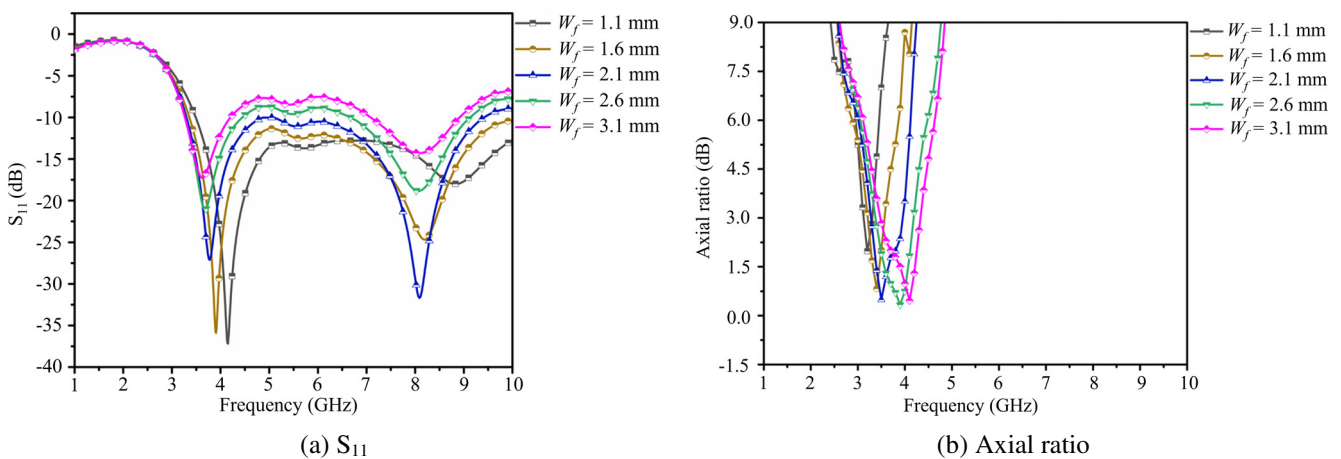


Fig. 17 Simulated results based on feed width variations

A feed width ( $W_f$ ) with parametric variation ranging from 1.1 mm to 3.1 mm was also performed. As the parameter  $W_f$  increased, the IPBW shifted towards the lower frequency side, along with a reduction in the matching (see Fig. 17). The ARBW tends toward higher frequencies along with enhancement. However, it was not enhanced beyond 3.1 mm because of the resonance-matching bandwidth reduction. The feed width of the design was optimized for 2.1 mm to compensate for the IPBW and ARBW. Furthermore, the inner and outer radius parameters were analyzed. As either the inner or outer radius varies, the circular polarization behavior was severely affected after a variation of one millimeter. This may be because this design was optimized from a basic annular ring. For any variation in radius, the feed length must be further optimized ( $L_g$ ).

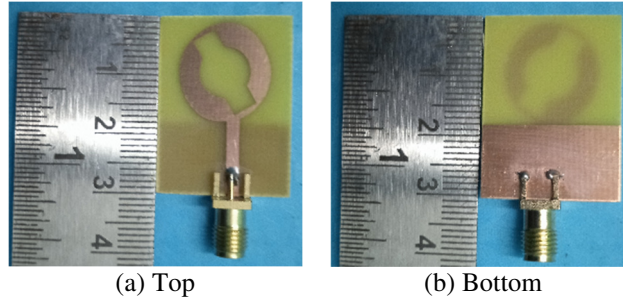


Fig. 18 Prototype of the proposed antenna

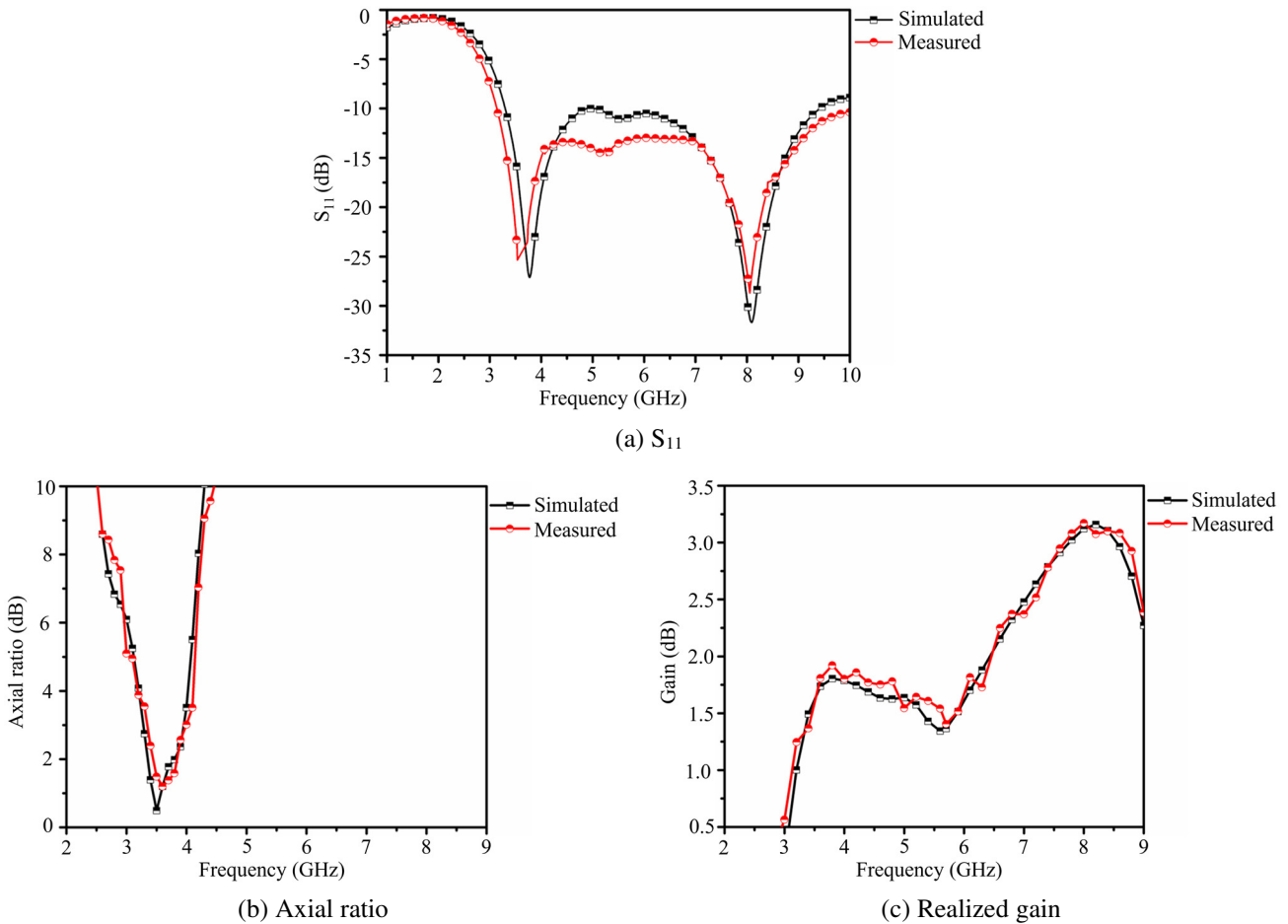


Fig. 19 Simulated and measured results

A prototype was fabricated to validate the design experimentally. Parameters such as  $S_{11}$ , AR, realized gain, and radiation pattern were measured. Fig. 18 shows the photography of the designed antenna. The  $S_{11}$  parameter was calculated using an Anritsu S820E vector network analyzer. Fig. 19(a) shows the simulated and measured results of  $S_{11}$ . The measured IPBW of the antenna achieved 104% with -10 dB of  $S_{11}$  and operated between 3.15 GHz to 10.0 GHz. The simulated IPBW was about 96.2% of the operating band between 3.30 GHz to 9.41 GHz. This may due to fabrication tolerances and measurement errors.

Fig. 19(b) shows the measured and simulated AR. The measured ARBW was similar to the simulated one with negligible deviation. The 3dB ARBW was observed at about 18.5% (3.3 GHz to 4 GHz). The minimum AR of the simulated and measured values were 0.4 dB at 3.5 GHz and 1.2 dB at 3.6 GHz. It was observed that the measured peak gain is 3.1 dBi at 8.1 GHz (see Fig. 19(c)). Simulated realized peak gain at 8.2 GHz was 3.2 dBi. A slight deviation of 0.1 was observed between the simulation and measurement. The gain varies from the lowest frequency to the highest frequency with an -10 dB IPBW and improved from a lower frequency to an upper frequency. The gain started degrading from 8.21 GHz.

Fig. 20 shows the simulated and measured radiation patterns in the elevation plane (E-plane or  $\phi = 0^\circ$ ) and the azimuth plane (H-plane or  $\phi = 90^\circ$ ) at 4.0 GHz, 6.0 GHz, and 8.0 GHz. As observed in the E-plane, the antenna radiated uniformly; whereas, in the H-plane, it radiated in a directional pattern at 4 GHz. Moreover, at the remaining frequencies, an almost omnidirectional pattern was observed in both planes except for a slight deviation at 8 GHz on the positive angle side. The proposed CP antenna design was compared with recent designs in the literature, both with and without the utilization of CMA. Compared to the literature presented in Table 2, the proposed antenna was more compact, except for the CPW-fed printed square slot antenna proposed by Jaiverdhan et al. [21]. However, this CPW-fed printed square slot antenna did not address the effect of feed length and substrate thickness required for obtaining circular polarization.

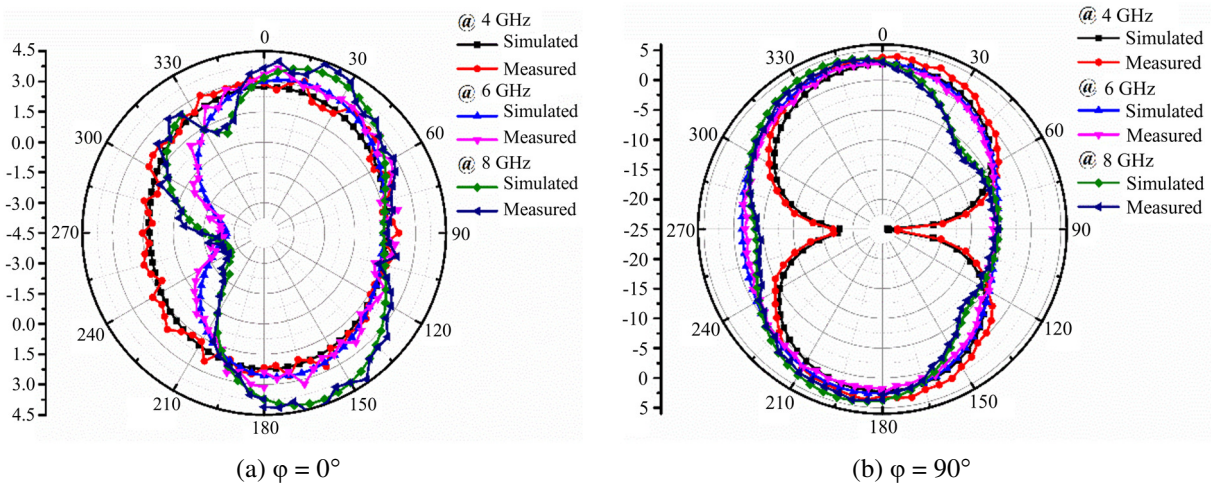


Fig. 20 Simulated and measured radiation patterns of 4,6 and 8 GHz

Table 2 Comparison of the proposed antenna with literature

Ref.	Antenna size $w \times l \times h$ (mm)	Impedance bandwidth		Axial ratio bandwidth		Peak gain (dBi)	CMA Yes/No
		%	GHz	%	GHz		
[10]	$79.2 \times 79.2 \times 1.52$	56.0	1.4-2.6	67	1.4-2.7	3.6	No
[11]	$44 \times 44 \times 1.6$	56.0	2.2-4.0	63.6	2.3-4.60	3.5	No
[12]	$33.5 \times 34.5 \times 1.6$	103	2.0-6.2	98	1.9-5.8	3.6	No
[13]	$20 \times 25 \times 0.8$	127	2-9	127	2-9	6.3	No
[19]	$45 \times 64 \times 1.1$	3.8	2.2-2.3	3.8	2.2-2.37	5.8	Yes
[21]	$20 \times 20 \times 1.524$	115	4-11	56	6.6-118	5.5	Yes
[22]	$50 \times 50 \times 0.4$	64.9	5.3-11	58.6	5.6-10.2	5.6	Yes
[23]	$42 \times 42 \times 1.524$	91	2.1-5.6	91	2.1-5.6	1.5	Yes
This study	$22 \times 30 \times 0.8$	104	3.1-10	18.5	3.3-4.0	3.2	Yes

## 5. Conclusions

This study uses a CMA systematic design approach to evaluate the proposed antenna design and achieve the Broad IPBW and circular polarization. A parametric study was conducted on the effects of feed width, substrate thickness, and ground plane length on antenna performance. The antenna prototype was then fabricated and experimentally tested. The measured IPBW

was 104% with -10 dB  $S_{11}$  and operated between 3.15 GHz to 10.0 GHz. The measured 3 dB ARBW was 18.5%, with the operating frequency between 3.3 GHz to 4.0 GHz. Both simulation and experimental results show that the proposed method exhibited excellent radiation properties with a gain of 3.1 dBi and a smaller size, making it easier to be integrated into printed circuit boards. In addition, it is suitable for various wireless applications, such as a sub-6 GHz 5G application band with circular polarization.

## Acknowledgments

This research was supported by the International Science and Technology Cooperation project of the Shenzhen Science and Technology Commission (GJHZ20200731095804014).

## Conflicts of Interest

The authors declare no conflict of interest.

## References

- [1] R. C. Han, S. S. Zhong, and J. Liu, "Broadband Circularly Polarised Dielectric Resonator Antenna Fed by Wideband Switched Line Coupler," *Electronics Letters*, vol. 50, no. 10, pp. 725-726, May 2014.
- [2] W. He, Y. He, and M. M. Tentzeris, "A Novel Wideband and Circularly Polarized Cross-Dipole Antenna," *Wireless Communications and Mobile Computing*, vol. 16, no. 17, pp. 3153-3162, December 2016.
- [3] G. Varshney, V. S. Pandey, R. S. Yaduvanshi, and L. Kumar, "Wide Band Circularly Polarized Dielectric Resonator Antenna with Stair-Shaped Slot Excitation," *IEEE Transactions on Antennas and Propagation*, vol. 65, no. 3, pp. 1380-1383, March 2017.
- [4] S. F. Seyyedrezaei, H. R. Hassani, M. Farahani, and S. Mohammad-Ali-Nezhad, "A Novel Small Size CPW-Fed Slot Antenna with Circular Polarization for 5G Application," *Progress in Electromagnetics Research C*, vol. 106, pp. 229-238, November 2020.
- [5] D. S. Chandu and S. S. Karthikeyan, "Broadband Circularly Polarized Printed Monopole Antenna with Protruded L-Shaped and Inverted L-Shaped Strips," *Microwave and Optical Technology Letters*, vol. 60, no. 1, pp. 242-248, January 2018.
- [6] T. Fujimoto, T. Ishikubo, and M. Takamura, "A Wideband Printed Elliptical Monopole Antenna for Circular Polarization," *IEICE Transactions on Communications*, vol. E100-B, no. 2, pp. 203-210, February 2017.
- [7] R. C. Han and S. S. Zhong, "Broadband Circularly-Polarised Chifre-Shaped Monopole Antenna with Asymmetric Feed," *Electronics Letters*, vol. 52, no. 4, pp. 256-258, February 2016.
- [8] K. Ding, C. Gao, Y. Wu, D. Qu, and B. Zhang, "A Broadband Circularly Polarized Printed Monopole Antenna with Parasitic Strips," *IEEE Antennas and Wireless Propagation Letters*, vol. 16, pp. 2509-2512, 2017.
- [9] H. Tang, K. Wang, R. Wu, C. Yu, J. Zhang, and X. Wang, "A Novel Broadband Circularly Polarized Monopole Antenna Based on C-Shaped Radiator," *IEEE Antennas and Wireless Propagation Letters*, vol. 16, pp. 964-967, 2017.
- [10] A. Panahi, X. L. Bao, G. Ruvio, and M. J. Ammann, "A Printed Triangular Monopole with Wideband Circular Polarization," *IEEE Transactions on Antennas and Propagation*, vol. 63, no. 1, pp. 415-418, January 2015.
- [11] M. Samsuzzaman, M. T. Islam, and M. J. Singh, "A Compact Printed Monopole Antenna with Wideband Circular Polarization," *IEEE Access*, vol. 6, pp. 54713-54725, 2018.
- [12] H. Alsariera, Z. Zakaria, and A. A. MISA, "New Broadband L-Shaped CPW-Fed Circularly Polarized Monopole Antenna with Asymmetric Modified Ground Plane and a Couple Series-Aligning Inverted L-Shaped Strip," *AEU - International Journal of Electronics and Communications*, vol. 118, article no. 153139, May 2020.
- [13] M. Manohar and A. K. Chaudhary, "Wideband Circularly Polarized Triangular Monopole Antenna for High-Speed Internet Access," *Journal of Electromagnetic Waves and Applications*, vol. 35, no. 15, pp. 2102-2113, 2021.
- [14] Y. Chen and C. F. Wang, *Characteristic Modes: Theory and Applications in Antenna Engineering*, New Jersey: Wiley, 2015.
- [15] V. Kollipara and S. Peddakrishna, "Enhancement of Higher Order Modes Using Characteristic Mode Analysis," 2nd International Conference on Artificial Intelligence and Signal Processing (AISP), pp. 1-4, February 2022.
- [16] B. Yang and J. J. Adams, "Computing and Visualizing the Input Parameters of Arbitrary Planar Antennas via Eigenfunctions," *IEEE Transactions on Antennas and Propagation*, vol. 64, no. 7, pp. 2707-2718, July 2016.

- [17] B. B. Q. Elias, P. J. Soh, A. A. Al-Hadi, P. Akkaraekthalin, and G. A. E. Vandenbosch, "A Review of Antenna Analysis Using Characteristic Modes," *IEEE Access*, vol. 9, pp. 98833-98862, 2021.
- [18] V. Kollipara and S. Peddakrishna, "Circularly Polarized Antennas Using Characteristic Mode Analysis: A Review," *Advances in Technology Innovation*, vol. 7, no. 4, pp. 242-257, October 2022.
- [19] Y. Chen and C. F. Wang, "Characteristic-Mode-Based Improvement of Circularly Polarized U-Slot and E-Shaped Patch Antennas," *IEEE Antennas and Wireless Propagation Letters*, vol. 11, pp. 1474-1477, 2012.
- [20] J. P. Ciafardini, E. A. Daviu, M. C. Fabres, N. M. Mohamed-Hicho, J. A. Bava, and M. F. Bataller, "Analysis of Crossed Dipole to Obtain Circular Polarization Applying Characteristic Modes Techniques," *IEEE Biennial Congress of Argentina (ARGENCON)*, pp. 1-5, June 2016.
- [21] J. Jaiverdhan, M. M. Sharma, R. P. Yadav, and R. Dhara, "Characteristic Mode Analysis and Design of Broadband Circularly Polarized CPW-Fed Compact Printed Square Slot Antenna," *Progress in Electromagnetics Research M*, vol. 94, pp. 105-118, 2020.
- [22] V. Kollipara and S. Peddakrishna, "Quad-Port Circularly Polarized MIMO Antenna with Wide Axial Ratio," *Sensors*, vol. 22, no. 20, article no. 7972, October 2022.
- [23] H. H. Tran, N. Nguyen-Trong, and A. M. Abbosh, "Simple Design Procedure of a Broadband Circularly Polarized Slot Monopole Antenna Assisted by Characteristic Mode Analysis," *IEEE Access*, vol. 6, pp. 78386-78393, 2018.
- [24] J. Bhattacharya and S. Maity, "A Comparative Study between Rectangular, Circular and Annular Ring Shaped Microstrip Antennas," *IEEE Calcutta Conference (CALCON)*, pp. 382-385, February 2020.
- [25] J. R. James and P. S. Hall, *Handbook of Microstrip Antennas*, 1st ed., London: Peter Peregrinus, 1989.
- [26] R. Xu, J. Y. Li, J. J. Yang, K. Wei, and Y. X. Qi, "A Design of U-Shaped Slot Antenna with Broadband Dual Circularly Polarized Radiation," *IEEE Transactions on Antennas and Propagation*, vol. 65, no. 6, pp. 3217-3220, June 2017.
- [27] O. Haraz and A. R. Sebak, "UWB Antennas for Wireless Applications," *Advancement in Microstrip Antennas with Recent Applications*, pp.125-152, March 2013.



Copyright© by the authors. Licensee TAETI, Taiwan. This article is an open access article distributed under the terms and conditions of the Creative Commons Attribution (CC BY-NC) license (<http://creativecommons.org/licenses/by/4.0/>).